International Journal of Heat and Fluid Flow 30 (2009) 579–589

Contents lists available at ScienceDirect

International Journal of Heat and Fluid Flow

journal homepage: www.elsevier.com/locate/ijhff

Direct numerical simulation of turbulent heat transfer in annuli: Effect of heat flux ratio

M. Ould-Rouiss *, L. Redjem-Saad, G. Lauriat

Université Paris-Est, Laboratoire de Modlisation et Simulation Multi Echelle (MSME FRE-CNRS 3160), 5 Bvd Descartes, Champs-sur-Marne, F-77454 Marne-la-Vallée Cedex 2, France

ARTICLE INFO

Article history:
Received 15 April 2008
Received in revised form 19 January 2009
Accepted 21 February 2009
Available online 3 April 2009

Keywords:
Direct numerical simulation (DNS)
Heat flux ratio effect
Turbulent heat transfer
Fully developed annular pipe flow

ABSTRACT

Fully developed turbulent flow and heat transfer in a concentric annular duct is investigated for the first time by using a direct numerical simulation (DNS) with isoflux conditions imposed at both walls. The Reynolds number based on the half-width between inner and outer walls, $\delta = (r_2 - r_1)/2$, and the laminar maximum velocity is $Re_\delta = 3500$. A Prandtl number $Pr = 0.71$ and a radius ratio $r^* = 0.1$ were retained. The main objective of this work is to examine the effect of the heat flux density ratio, $q^* = q_1/q_2$, on different thermal statistics (mean temperature profiles, root mean square (rms) of temperature fluctuations, turbulent heat fluxes, heat transfer, etc.). To validate the present DNS calculations, predictions of the flow and thermal fields with $q^* = 1$ are compared to results recently reported in the archival literature. A good agreement with available DNS data is shown. The effect of heat flux ratio q^* on turbulent thermal statistics in annular duct with arbitrarily prescribed heat flux is discussed then. This investigation highlights that heat flux ratio has a marked influence on the thermal field. When q^* varies from 0 to 0.01, the rms of temperature fluctuations and the turbulent heat fluxes are more intense near the outer wall while changes in q^* from 1 to 100, lead to opposite trends.

1. Introduction

A literature review reveals that the mechanism of turbulent flow and heat transfer in annular ducts is far from being understood, and that investigations of the thermal interferences between inner and outer walls and their impact upon the convective heat transfer is very scarce. Many theoretical analysis and experimental studies have been devoted to this kind of geometry because of the numerous engineering applications (heat exchangers, cooling or electric devices, nuclear reactors, etc.).

Kays and Leung (1963) gave a review of the previous experimental studies. In 1963, these authors published the most reliable numerical analysis of broad scope up till now. Their paper addresses the problem of turbulent flow and heat transfer in a concentric circular tube annulus with fully developed velocity profile and constant heat rate per unit of length. Asymptotic solutions were developed for various ranges of radius ratio, Reynolds number and Prandtl number. A superposition method was used for solving the problem of asymmetric heating from the two surfaces of an annulus.

Most of prior numerical investigations, including that of (Kays and Leung, 1963) are subjected to considerable errors because of the use of the eddy viscosity model to represent the time-averaged turbulent shear stress, and in many cases, incoherent and inaccurate expressions for that heuristic quantity leading to highly inaccurate time-averaged velocity distribution (Yu et al., 2005a). Recently, Yu et al. (2005a) derived new numerical solutions for the Nusselt number for fully developed turbulent convection in an annulus uniformly heated on the inner wall and adiabatic outer wall. They pointed out that their study was conducted on the basis of theoretical considerations (the numerical solutions were based on integration of the differential energy balance using an empirical expression for the local fraction of the radial transport of energy due to turbulence) which are more accurate numerically and practically functionally than any prior ones. They concluded that the available experimental data appear to confirm their assertions, but because of their limited scope and differences from set to set, they did not provide a critical test of their new predictions.

Yu et al. (2005b) computed solutions with the same model for different thermal boundary conditions: (1) uniform heating on the outer surface only, (2) equal uniform heat fluxes on the two surfaces and (3) uniform heating on one surface with equal cooling on the other. The predicted values of Nusselt number are in good agreement with the somewhat limited experimental data.

Zeng et al. (2007) reviewed the few recent experimental investigations on forced flow and heat transfer with water in bilaterally heated narrow annular ducts. They focused their theoretical analysis on the characteristics of the flow and convective heat transfer on the conditions of both developed laminar and turbulent flows. Their mathematical model combines the time-averaged partial differential equation for the conservation of energy in the radial

* Corresponding author.
E-mail address: ould@univ-mlv.fr (M. Ould-Rouiss).

0142-727X/$ - see front matter © 2009 Elsevier Inc. All rights reserved.
doi:10.1016/j.ijheatfluidflow.2009.02.018

Nomenclature

C_p	specific heat capacity
D_h	equivalent hydraulic diameter $2(r_2 - r_1)$
h_j	heat transfer coefficient at surface j
k	thermal conductivity
L	length of the computational domain
Nu_j	Nusselt number at surface $j, Nu = h_j D_h/k$
Pr	Prandtl number, $Pr = \nu/\alpha$
q_j	heat flux density at surface j
q^*	heat flux ratio $q^* = q_1/q_2$
Re	Reynolds number $Re = U_l\delta/\nu$
r	dimensionless coordinate in radial direction scaled by δ
r^*	radius ratio $r^* = r_1/r_2$
T	temperature
T_b	bulk temperature
T_r	reference temperature, $T_r = q_r\delta/k$
T_w	wall temperature
T_τ	friction temperature, $T_\tau = q_w/\rho C_p u_\tau$
$u,\ v$	axial and radial velocity components
u_τ	friction velocity
U_b	bulk velocity
U_l	maximum velocity of the laminar flow
y^+	distance from the wall in viscous wall units
z	coordinate in axial direction

Greek letters

δ	half gap width, $\delta = (r_2 - r_1)/2$
θ	coordinate in circumferential direction
Θ	dimensionless temperature, $\Theta = (\langle T_w\rangle - T)/T_r$
ν	kinematic viscosity
ρ	specific density

Superscripts

$\overline{()}$	statistically averaged
+	normalized by u_τ, ν and T_τ
$'$	fluctuation component
1	inner wall
2	outer wall

direction in fully developed convection with an overall energy balance. The radial heat flux density due to turbulence and the shear stress are based on numerically modified empirical correlations. Under turbulent flow conditions, they found that the decrease of the gap size yields heat transfer deterioration on the inner wall while it enhances the heat transfer on the outer wall.

It is worth noting that all prior numerical analysis are not free of empiricism, quite limited in scope and thus uncertain in results. Moreover, all these prior numerical analysis have derived only the heat transfer coefficient (Nusselt number). Direct Numerial Simultions (DNS) are free of the sources of errors present in prior numerical analysis. With DNS, one can derive more turbulence statistics (mean velocity and temperature profiles, root mean squares of velocity and temperature fluctuations, radial and axial heat fluxes, etc.). The present work is the first DNS which investigates the effects of heat flux ratio on turbulent heat transfer in annular pipe flows under isoflux wall condition. The motivation of this work is to deal with the characteristics of the fully developed turbulent air flow and heat transfer in bilaterally heated annular duct as illustrated in Fig. 1.

In Section 2 of the present paper, the formulation of the problem and the numerical method are given. To validate our code, DNS on turbulent flow (accurate predictions of the flow field being a prerequisite for correct predictions of the heat transfer) and heat transfer in case of uniform equal heating of both surfaces has been carried out (Section 3), and showed good agreement with available DNS data of literature (Chung and Sung, 2003). The effect of heat flux ratio, $q^* = q_1/q_2$ (ratio of heating flux at the inner wall of annulus to that at the outer wall), on the different thermal statistics (mean temperature profiles, root mean square of fluctuating temperature, radial and axial heat fluxes) is investigated and discussed in Section 3. Conclusions in Section 4 ends this work.

2. Governing equations and numerical method

Fig. 1 depicts the annular flow configuration investigated. The turbulent flow is fully developed and the newtonian fluid is incompressible (Prandtl number $Pr = 0.71$). At the inner and outer walls,

Table 1
Grid resolutions compared to those of Chung and Sung (2003).

	DNS	Chung and Sung (2003)
N_θ	257	256
N_r	65	65
N_z	257	192
$L^+_{\theta_i}$	249.93	250.28
$L^+_{\theta_e}$	2499.31	1975.57
L^+_z	4475	2688.75
$r_i\Delta\theta^+$	0.97	0.98
$r_e\Delta\theta^+$	9.72	7.72
Δr^+_i	0.107	0.15
Δr^+_e	0.09	0.12
Δr^+_{max}	8.7	15.23
Δz^+	17.4	14

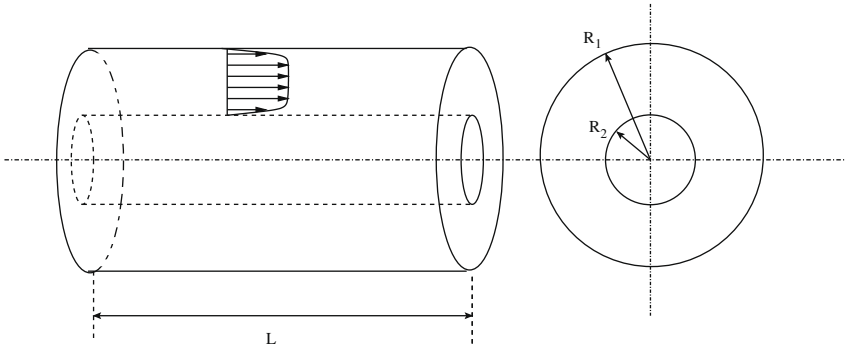

Fig. 1. Schematic of the computational domain.

uniform heat fluxes q_1 and q_2 are, respectively, imposed. The fluid properties are assumed constant and the viscous dissipation term is neglected. Therefore, temperature may be considered as a passive scalar. The dimensionless temperature Θ is defined as:

$$\Theta = (\langle T_b \rangle - T)/T_r \tag{1}$$

where $T_r = q_e\delta/k$ is the reference temperature, and $q_e = q_2 + r^* q_1$.

$\langle T_b \rangle$ denotes the bulk temperature averaged in time and circumferential direction. Using the dimensionless variables $q_r = r \cdot v_r,\ q_\theta = r \cdot v_\theta,\ q_z = v_z$, the governing equations (continuity, momentum and energy equations) write as follow:

$$\frac{1}{r}\frac{\partial}{\partial r}(q_r) + \frac{1}{r}\frac{\partial}{\partial \theta}(q_\theta) + \frac{\partial}{\partial z}(q_z) = 0 \tag{2}$$

$$\frac{Dq_r}{Dt} = -r\frac{\partial p}{\partial r} + \frac{1}{Re}\left[r\frac{\partial}{\partial r}\left(\frac{1}{r}\frac{\partial q_r}{\partial r}\right) + \frac{1}{r^2}\frac{\partial^2 q_r}{\partial \theta^2} + \frac{\partial^2 q_r}{\partial z^2} - \frac{2}{r}\frac{\partial q_\theta}{\partial \theta}\right] \tag{3}$$

$$\frac{Dq_z}{Dt} = \frac{\partial p}{\partial z} + \frac{1}{Re}\left[\frac{1}{r}\frac{\partial}{\partial r}\left(r\frac{\partial q_z}{\partial r}\right) + \frac{1}{r^2}\frac{\partial^2 q_z}{\partial \theta^2} + \frac{\partial^2 q_z}{\partial z^2}\right] \tag{4}$$

$$\frac{Dq_\theta}{Dt} = -\frac{1}{r}\frac{\partial p}{\partial \theta} + \frac{1}{Re}\left[\frac{\partial}{\partial r}r\frac{\partial}{\partial r}\left(\frac{q_\theta}{r}\right) - \frac{q_\theta}{r^2} + \frac{1}{r^2}\frac{\partial^2 q_\theta}{\partial \theta^2} + \frac{\partial^2 q_\theta}{\partial z^2} + \frac{2}{r^3}\frac{\partial q_r}{\partial \theta}\right] \tag{5}$$

with

$$\frac{Dq_r}{Dt} = \frac{\partial q_r}{\partial t} + \frac{\partial}{\partial r}\left(\frac{q_r q_r}{r}\right) + \frac{\partial}{\partial \theta}\left(\frac{q_r q_\theta}{r}\right) + \frac{\partial}{\partial z}(q_r q_z) - q_\theta q_\theta \tag{6}$$

$$\frac{Dq_z}{Dt} = \frac{\partial q_z}{\partial t} + \frac{1}{r}\frac{\partial}{\partial r}(q_r q_z) + \frac{1}{r}\frac{\partial}{\partial \theta}(q_\theta q_z) + \frac{\partial}{\partial z}(q_z q_z) \tag{7}$$

$$\frac{Dq_\theta}{Dt} = \frac{\partial q_\theta}{\partial t} + \frac{1}{r^2}\frac{\partial}{\partial r}(r q_r q_\theta) + \frac{1}{r}\frac{\partial}{\partial \theta}(q_\theta q_\theta) + \frac{\partial}{\partial z}(q_\theta q_z) \tag{8}$$

$$\frac{\partial \Theta}{\partial t} + \frac{1}{r}\frac{\partial}{\partial r}(q_r\Theta) + \frac{1}{r}\frac{\partial}{\partial \theta}(q_\theta\Theta) + \frac{\partial}{\partial z}(q_z\Theta) - q_z\frac{\partial}{\partial z}\left(\frac{\langle T_b \rangle_\theta}{T_r}\right) = \frac{1}{Re.Pr}\left[\frac{1}{r}\frac{\partial}{\partial r}\left(r\frac{\partial \Theta}{\partial r}\right) + \frac{1}{r^2}\frac{\partial^2 \Theta}{\partial \theta^2} + \frac{\partial^2 \Theta}{\partial z^2}\right] \tag{9}$$

where r and the velocity components are scaled by the half of the gap width, δ, and maximum velocity of the laminar profile, U_l, respectively. The Reynolds number Re is defined as $Re = Re_\delta = U_l\delta/\nu$.

The heating condition imposed on the walls implies a linear increase of the bulk temperature $\langle T_b \rangle$ in the streamwise direction. For fully developed flows, the following equalities are satisfied:

$$\frac{\partial \langle T \rangle_\theta}{\partial z} = \frac{\partial \langle T_b \rangle_\theta}{\partial z} = \frac{\partial \langle T_{w2} \rangle_\theta}{\partial z} = \frac{\partial \langle T_{w1} \rangle_\theta}{\partial z} = \frac{2(r_1 q_1 + r_2 q_2)}{\rho C_p U_b (r_2^2 - r_1^2)} \tag{10}$$

where $\langle T_{w_1} \rangle$ and $\langle T_{w_2} \rangle$ are the inner wall and outer wall temperatures averaged in time and circumferential direction. The boundary conditions are given as:

- At the inner wall:

$$r = 2r^*/(1 - r^*) \rightarrow \frac{\partial \Theta}{\partial r} = q^*/(1 + q^* r^*)$$

- At the outer wall:

$$r = 2/(1 - r^*) \rightarrow \frac{\partial \Theta}{\partial r} = 1/(1 + q^* r^*)$$

The governing equations were discretized on a staggered mesh in cylindrical coordinates with a computational length in the axial direction $L = 25\delta$. The numerical integration was performed by a finite difference scheme, second-order accurate in space and in time. The time advancement employed a fractional step method.

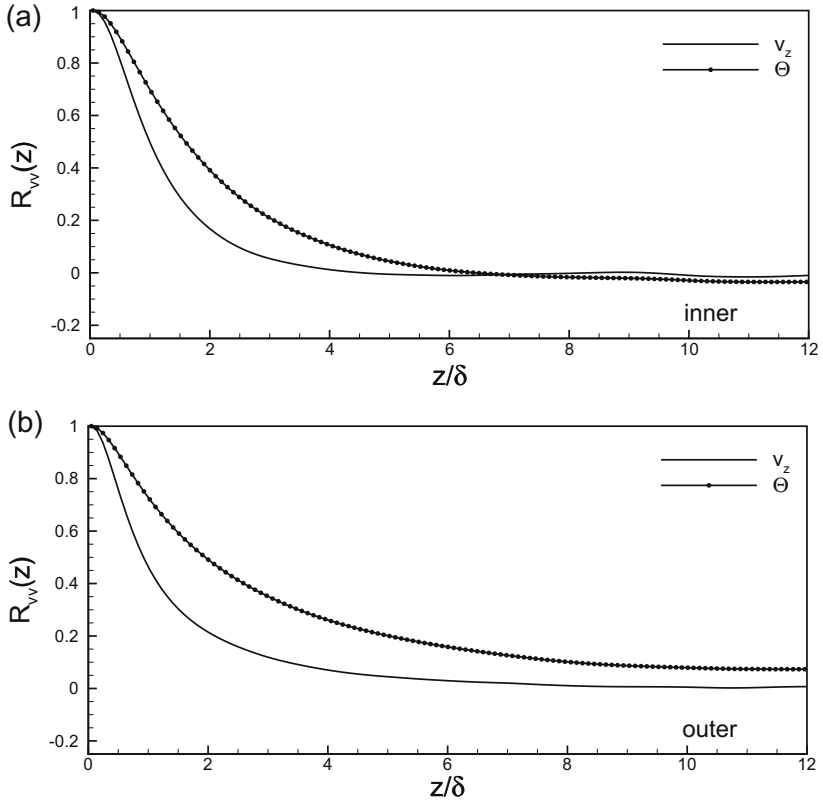

Fig. 2. Two-point correlations in the axial direction.

A third-order Runge–Kutta explicit scheme and a Crank–Nicolson implicit scheme were used to evaluate the convective and diffusive terms, respectively. Uniform computational grid and periodic boundary conditions were applied to the circumferential and axial directions. No-slip boundary conditions are applied on the walls. Computations were carried out on $(N_\theta \times N_r \times N_z) = (257 \times 65 \times 257)$ grid. For $q^* = 1$, Table 1 compares the different informations concerning the grid resolution to those of Chung and Sung (2003). The above grid was found to provide an accurate prediction of turbulence statistics (in agreement with the available data of literature) and to give a good compromise between the required CPU-time and accuracy. The time is made dimensionless using the half gap width, δ, and the maximum velocity of the laminar flow, U_l. The calculations have been conducted at constant CFL (Courant, Friedrichs and Lewy condition, CFL = 1.7). In this case, the time step is computed from the imposed CFL, which is however limited by the value $0.08\delta/U_l$ in order to avoid large time discretization errors.

To ensure that the computational domain used in the present study is adequate to capture the largest thermal structures, we have analyzed the two-point correlations of the fluctuating streamwise velocity and temperature, as can be seen in Figs. 2 and 3, in the axial and azimuthal directions, respectively, at the distance $y^+ \simeq 5$ from inner and outer walls. In the axial direction, Fig. 2 shows that the auto-correlation of the fluctuating streamwise velocity tends to zero, meaning that the computational domain is large enough to simulate the largest eddies in the flow. Near the outer wall, the fluctuating temperature does not decay to zero; its value remains constant and equal to 0.07. This observation has been also reported by Chung and Sung (2003) with a constant value equal to 0.09. The auto-correlation of the fluctuations of temperature does not vanish. In their DNS, and with similar boundary conditions (isoflux boundary conditions), Tiselj et al. (2001) showed that the auto-correlation of fluctuating temperature does not vanish for this kind of boundary conditions even if the domain is enlarged. They pointed out that a large enough domain (in the periodic directions) to capture the largest eddies in the flow is also large enough for the scalar field. The two-point correlations in the azimuthal direction (Fig. 3) fall off to zero at both walls. There is a slight deviation between the negative peaks of fluctuating temperature and axial velocity, due to the difference in the boundary conditions for the temperature field (isoflux boundary conditions) and the velocity field (no-slip boundary conditions).

3. Results and discussion

3.1. Mean velocity profile

To validate the present study, predictions are compared to the DNS data of Chung et al. (2002). Fig. 4a illustrates the mean streamwise velocity profile normalized by the bulk velocity, U_b, along with the DNS data of Chung et al. (2002). The comparison between the two profiles exhibits a surprisingly good agreement between them. The mean streamwise velocity profiles scaled by the inner friction velocity, $u_{\tau 1}$, and the outer friction velocity, $u_{\tau 2}$, display the different regions of the flow near the walls (Fig. 4b). At the outer tube, one can clearly distinguish: the viscous sublayer, $0 \leqslant y^+ \leqslant 5$, with a linear law for the velocity profile; the buffer region, $5 < y^+ \leqslant 30$, and the logarithmic region which extends up to $y^+ \simeq 200$ and where the profile develops as $v_z^+ = 2.5 \ln(y^+) + 5.5$. At the inner wall, the viscous sublayer is clearly seen. From $y^+ \simeq 5$, a slight deviation between the inner and outer walls is ob-

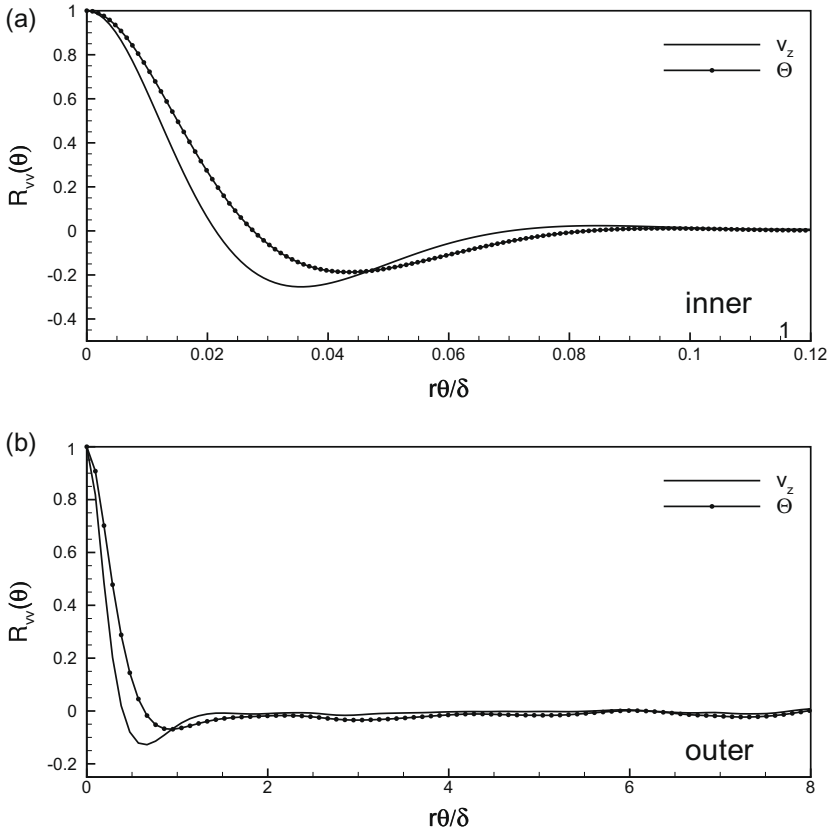

Fig. 3. Two-point correlations in the azimuthal direction.

served. The difference is significant in the logarithmic region where the velocity profile deviates from the log law. This is attributed to the curvature effect near the inner cylinder. Chung et al. (2002) showed that the inner profile tends to the outer one (and follows a logarithmic law) when the radius ratio increases. Due to the curvature effects, the friction coefficient ($C_f = 2\tau_w/\rho U_b$) of the inner tube ($C_{f_1} = 0.01314$) is larger than that of the outer one ($C_{f_2} = 0.00837$), in accordance with Chung et al. (2002) findings ($C_{f_1} = 0.01300$ and $C_{f_2} = 0.00810$).

3.2. Root mean square velocity fluctuations

The root mean square (rms) velocity fluctuations nondimensionalized by friction velocity are given in Fig. 5 along with the DNS results by Chung et al. (2002). The predicted fluctuations in the streamwise (Fig. 5a) wall-normal (Fig. 5b) and azimuthal (Fig. 5c) directions show an excellent agreement with the DNS data of Chung et al. (2002). The velocity fluctuations close to the inner wall are smaller than those at the outer wall, owing to the transverse curvature effect. This difference in the values of the velocity fluctuations at the inner and outer cylinders is reduced with an increase in the radius ratio. Indeed, the velocity fluctuations in the plane channel have the same behavior near both walls. In the annular space with a small radius ratio, the surface of the inner tube is smaller than the one of the outer tube, and thus supplies less turbulent kinetic energy. The maximum in the streamwise velocity fluctuations close to the inner and outer walls occurs at

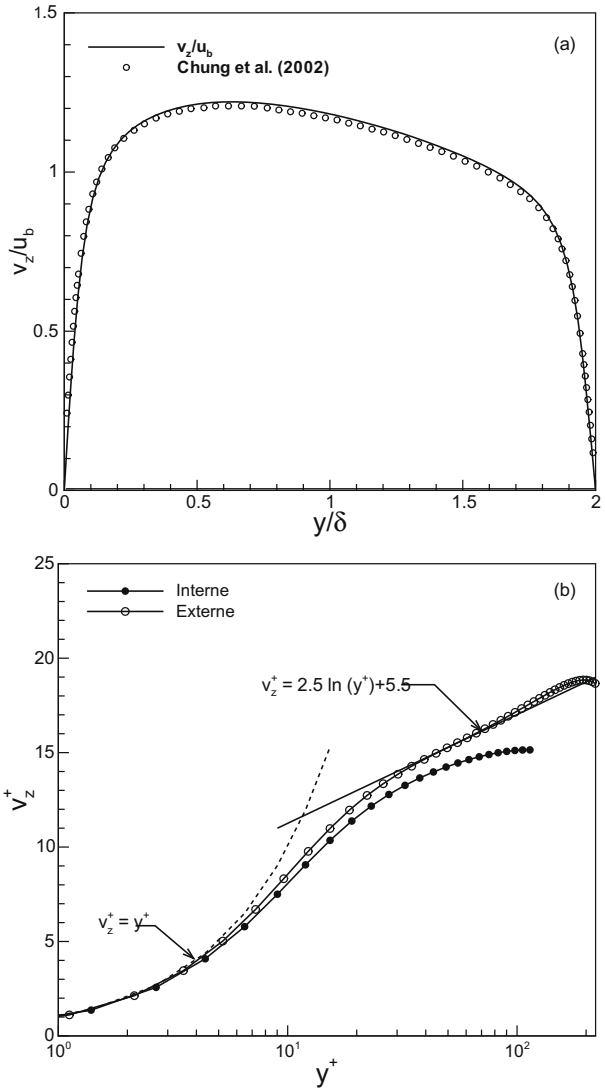

Fig. 4. Mean velocity profile.

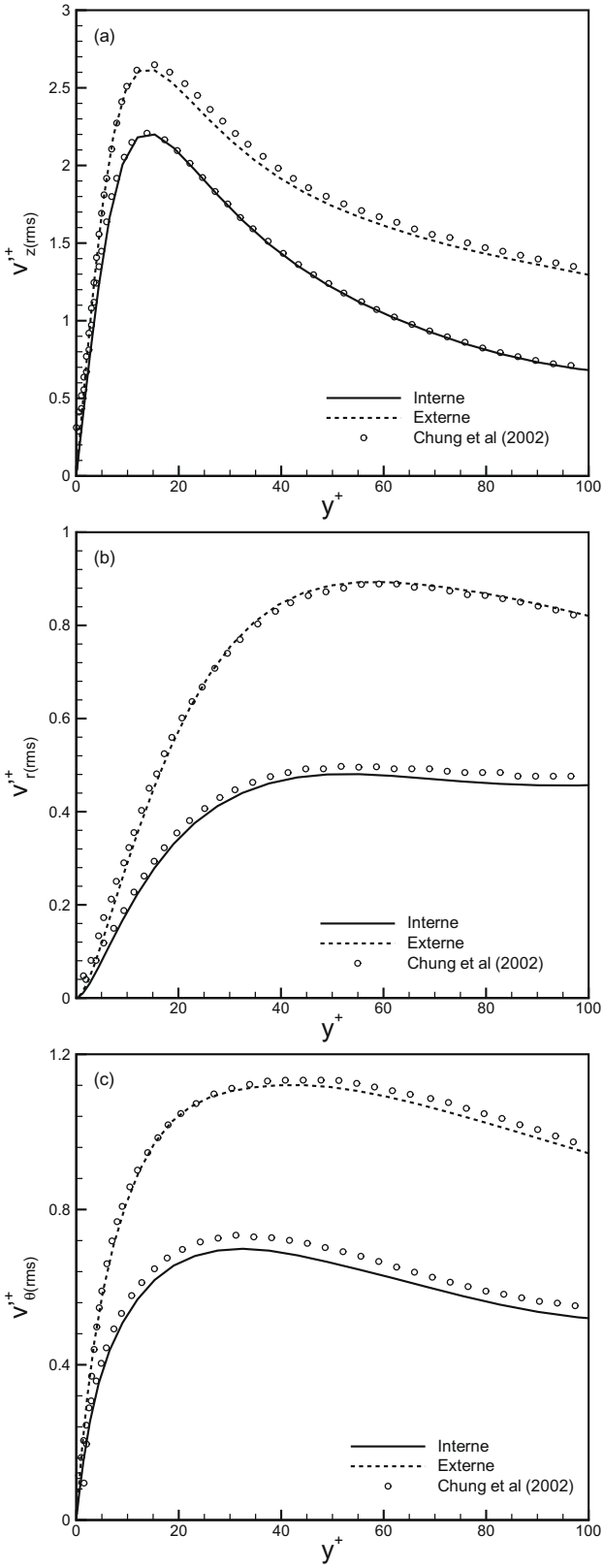

Fig. 5. RMS velocity fluctuations: (a) streamwise, (b) radial and (c) azimuthal.

the distance $y^+ \simeq 14$. The value of the peak is $v_z'^+ = 2.2$ for the inner side and $v_z'^+ = 2.6$ for the outer side. The latter value (2.6) is also found in the plane channel flow (Kim et al., 1987) as well as in the cylindrical pipe flow (Redjem-Saad (2008)) where the peak in the streamwise velocity fluctuations is also located at $y^+ \simeq 14$. This is a further indication that the radius ratio has no effect on the peak in the streamwise velocity fluctuations at both walls. It is interesting to note that the flow geometry also has no effect on the peak value near the outer cylinder. However, the value close to the inner wall seems to be affected by the flow geometry. Chung et al. (2002) reported that with increases in the radius ratio, this peak rises in the vicinity of inner wall and tends to the value $v_z'^+ = 2.6$. Similar behavior is observed for the two other velocity components. The small turbulence intensity of the radial and azimuthal velocities at the inner tube is caused by the curvature effects.

3.3. Turbulent shear stresses

Fig. 6 compares the position of maximum velocity (Fig. 6a) and the position of zero total shear stress (Fig. 6b). In Fig. 6b, the radial profiles of the Reynolds shear stress ($\overline{v_r' v_z'}$) as well as the total shear stress ($-\overline{v_r' v_z'} + (1/Re)(dv_z/dy)$) are scaled by the friction velocity $u_{\tau 1}$, and plotted versus the distance from the inner wall. The pipe's walls being at rest, $\overline{v_r' v_z'}$ is the only non zero turbulent shear stress. The Reynolds shear stress $\overline{v_r' v_z'}$ is asymmetric like the velocity profile for which the maximum is close to the inner wall, at $y/\delta = 0.64$ as shown in Fig. 6a. Note that the position of the total shear stress does not match with the position of the maximum velocity. The position of the total shear stress is closer to the inner wall and is located at $y/\delta = 0.61$. The total and Reynolds shear stresses are non-linear, especially in the vicinity of the wall regions. Moreover, the Reynolds shear stress near the outer tube is more intense than that near the inner tube. The present predictions agree fairly well with the DNS findings of Chung et al. (2002).

3.4. Mean temperature profiles

Fig. 7 depicts the mean temperature distributions nondimensionalized by the friction temperature of each wall, versus the distance to the inner or outer annulus wall for various heat flux ratios $q^* = q_1/q_2$. In the vicinity of the inner cylinder, Fig. 7a, the well known asymptotic behavior $\Theta^+ = Pr \cdot y^+$ is observed in the viscous sublayer, irrespective of the heat flux ratio. Beyond this sublayer, the turbulent heat transfer in the annular duct is clearly affected by the heat flux ratio. Heat transfer at the inner wall is less important when the heat flux ratio decreases. For the smallest value of heat flux ratio, $q^* = 0.01$, the buffer region as well as the logarithmic one are practically non-existent. For the highest heat flux ratio, $q^* = 100$, the buffer region can be better distinguished and the logarithmic part of the temperature profile extends further.

On the contrary, Fig. 7b shows that the turbulent heat transfer at the outer wall increases with decreases in q^*. The logarithmic zone in the temperature profile extends more when the heat flux ratio is reduced. The outer temperature profile is significantly affected for the highest q^*-value ($q^* = 100$), and the logarithmic region totally disappears. It should be noted that for a given heat flux ratio, the inner and outer temperature profiles are appreciably different. Chung and Sung (2003) reported the same observation and showed that the deviation between the inner and outer temperature profiles is more pronounced for the radius ratio $r^* = 0.1$ than that for $r^* = 0.5$, due to a stronger curvature effects.

3.5. Root mean square of temperature fluctuations

Fig. 8 depicts the root mean square (rms) profile of temperature fluctuations normalized by the friction temperature of each wall,

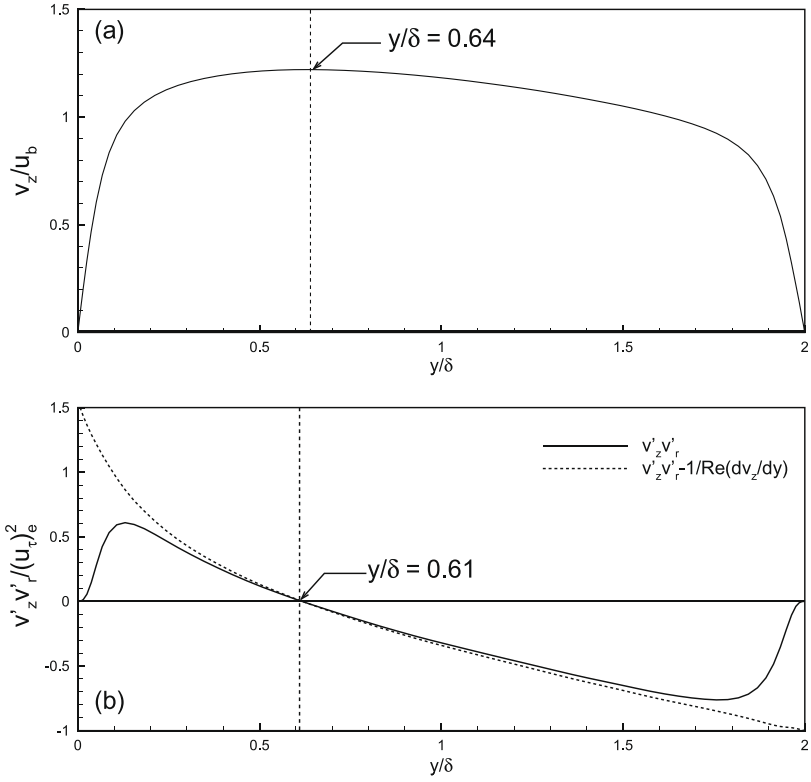

Fig. 6. Positions of zero total shear stress r_0 and maximum velocity r_{max}.

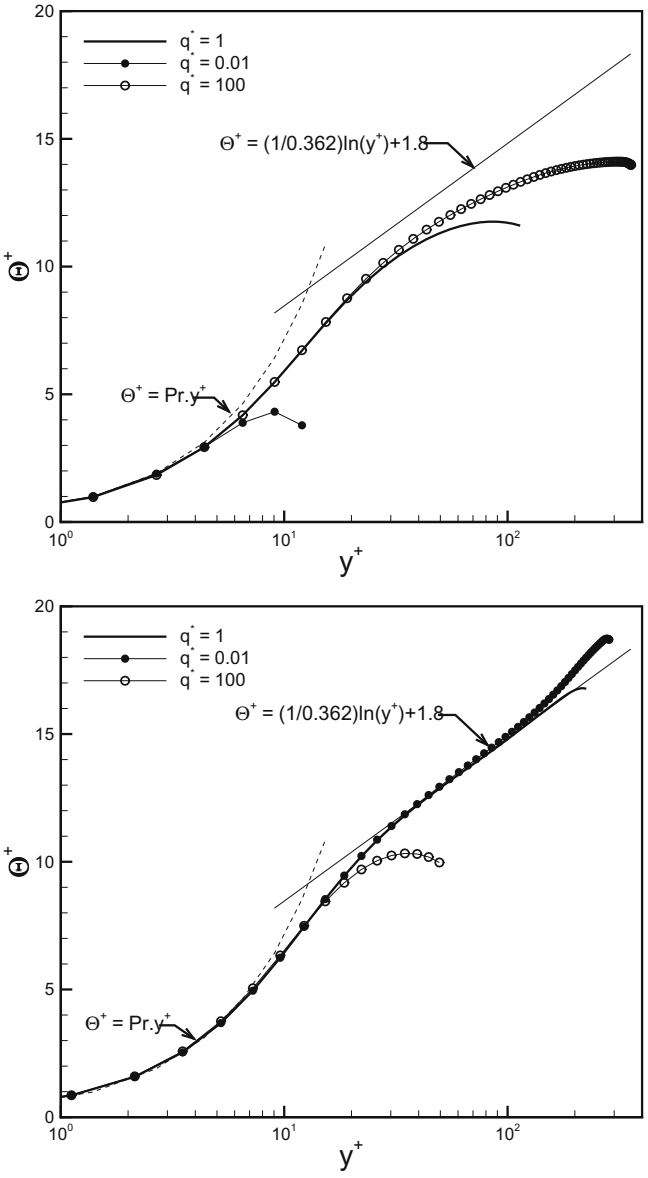

Fig. 7. Mean temperature profiles. (a) inner cylinber and (b) outer cylinder.

for $q^* = 1$. The present DNS predictions are in accordance with the findings of literature. At the inner wall, the agreement is remarquably good; at the outer wall, the rms of fluctuating temperature is slightly underestimated in comparison to the rms obtained by Chung and Sung (2003), in the region $y^+ > 10$, which may be due to the different grid size in the radial direction (Table 1). In the present DNS, a cosine function is used for clustering the grid points in the radial direction and the grid size in the wall-normal direction is thinner than that used by Chung and Sung (2003).

Because of the curvature effects, the intensity of the temperature fluctuations at the outer cylinder is larger than that at the inner cylinder. The peaks of the temperature fluctuations are located at the same distance from the walls, $y^+ \simeq 14$, which coincides with the position of the peaks of axial velocity fluctuations shown by Redjem-Saad (2008). Unlike the results found for the pipe flow (Redjem-Saad et al. (2007)), the rms of temperature fluctuations in the annular space does not vanish as the wall is approached. This difference is attributed to the different boundary conditions in pipe and annular flows. In the pipe flow, a mixed condition is imposed ($\Theta^+ = 0$) which implies that the temperature fluctuations vanish at the wall. In the annular flow, these fluctuations are not zero at the walls, since isoflux boundary conditions are imposed. The rms of temperature fluctuations at the outer tube is equal to 2.2, irrespective of the geometry flow. In the literature, this value is generally found between 2 and 2.2 (Lu and Hetsroni, 1995; Kong et al., 2000; Tiselj et al., 2001). In the region $y^+ > 20$, in the vicinity of the outer surface, Θ'^+_{rms} coincides with that for the pipe flow, because of the small radius ratio ($r^* = 0.1$).

The root mean square fluctuations normalized by the bulk temperature are plotted for a wide range of heat flux ratios, $q^* \leqslant 1$ (Fig. 9a) and $q^* \geqslant 1$ (Fig. 9b). When investigating the fully developed turbulent flow in concentric annuli, it has been established that the distribution of velocity fluctuations display smaller turbulence intensities near the inner wall, in comparison to those in the vicinity of the outer wall. Since the surface of the inner tube is smaller than the outer wall surface, the inner wall supplies relatively less turbulent kinetic energy. Similarly, for the heat flux ratio $q^* = 1$, the temperature fluctuation intensity is more important near the outer wall of annulus than at the inner wall. The surface of the outer cylinder is larger than the inner wall surface, and produces more heat. This trend is observed only for the heat flux ratios $q^* \leqslant 1$. For $q^* > 1$, the opposite is seen: the fluctuating inner temperatures surpass the fluctuating outer temperatures, and this

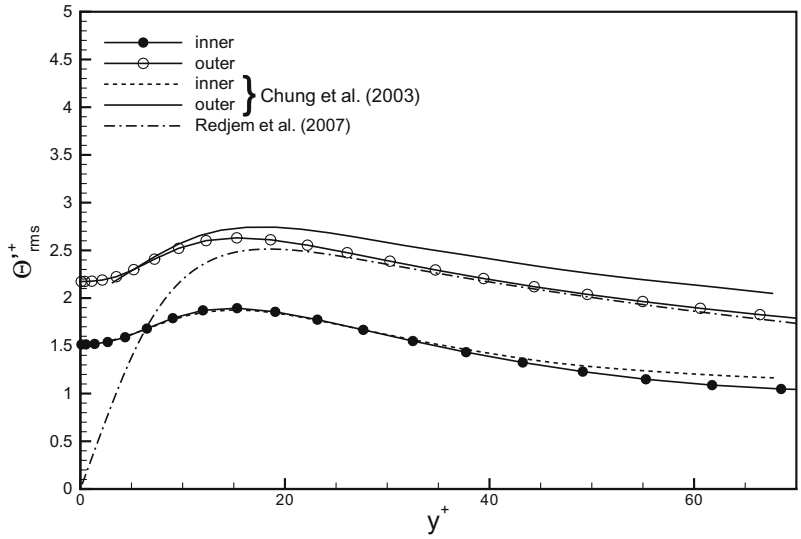

Fig. 8. RMS of temperature fluctuations for $q^* = 1$.

difference is more apparent when increasing the heat flux ratio. An increase in heat flux ratio, $q^* = q_1/q_2$, (from 1 to 100) means indeed that the increase in the heat flux at the inner wall of the annulus, q_1, is more pronounced and more important than that at the outer wall, q_2. Bringing more heat flux at the smaller surface compensates the difference between the two walls. Note that for $q^* \simeq 2$, Fig. 9b shows a nearly symmetric distribution of the temperature rms. Imposing more and more heat flux at the inner wall leads to larger fluctuating inner temperature, when $q^* \to 100$ (even if the outer wall supplies more turbulent kinetic energy than the inner one). This suggests that the flow field has less impact on the temperature field when $q^* \gg 1$ than it has in the case $q^* \leqslant 1$ (for which a strong similarity exists between the flow and thermal fields).

At both the inner and outer walls, the peak of the temperature fluctuations is always located at the same position, irrespective of the value of heat flux ratio. The effect of heat flux ratio on the magnitude of the peak in the rms profiles is very marked close to the inner wall, as can be seen in Fig. 9a and b shows that it is more pronounced for $q^* > 1$. When q^* decreases from 1 to 0.01, the temperature fluctuation level reduces near the inner wall. The peak disappears for $q^* < 0.5$, while the temperature fluctuation level slightly increases in the vicinity of the outer cylinder. When q^* varies from 1 to 100, the peak remains distinct near the two cylinders. For $q^* = 100$, it disappears near the outer wall, whereas the temperature fluctuation intensity is significantly enhanced near the inner wall.

3.6. Turbulent heat fluxes

The streamwise and wall-normal turbulent heat fluxes normalized by the friction velocity and friction temperature are displayed for $q^* = 1$ in Fig. 10a and b, respectively. The turbulent heat fluxes near the outer wall are larger than those near the inner one, like the rms profile of temperature fluctuations. There is a good agreement between our calculations and the DNS data by Chung and Sung (2003), despite a small discrepancy at the outer wall for $y^+ > 20$. The turbulent heat fluxes obtained for a pipe flow (Redjem-Saad et al. (2007)) are also depicted in Fig. 10. The radius ratio being small ($r^* = 0.1$), the present predictions near the outer wall behave as turbulent heat fluxes for a pipe flow.

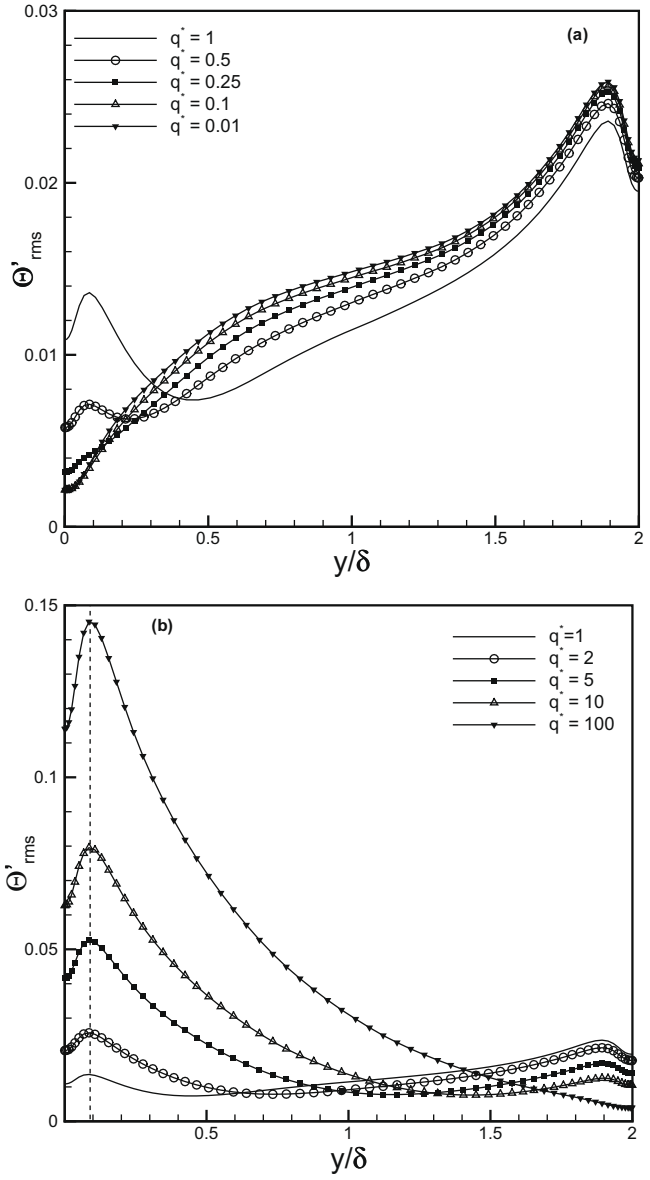

Fig. 9. RMS of temperature fluctuations for various heat flux ratios. (a) $q^* \leqslant 1$ and (b) $q^* \geqslant 1$.

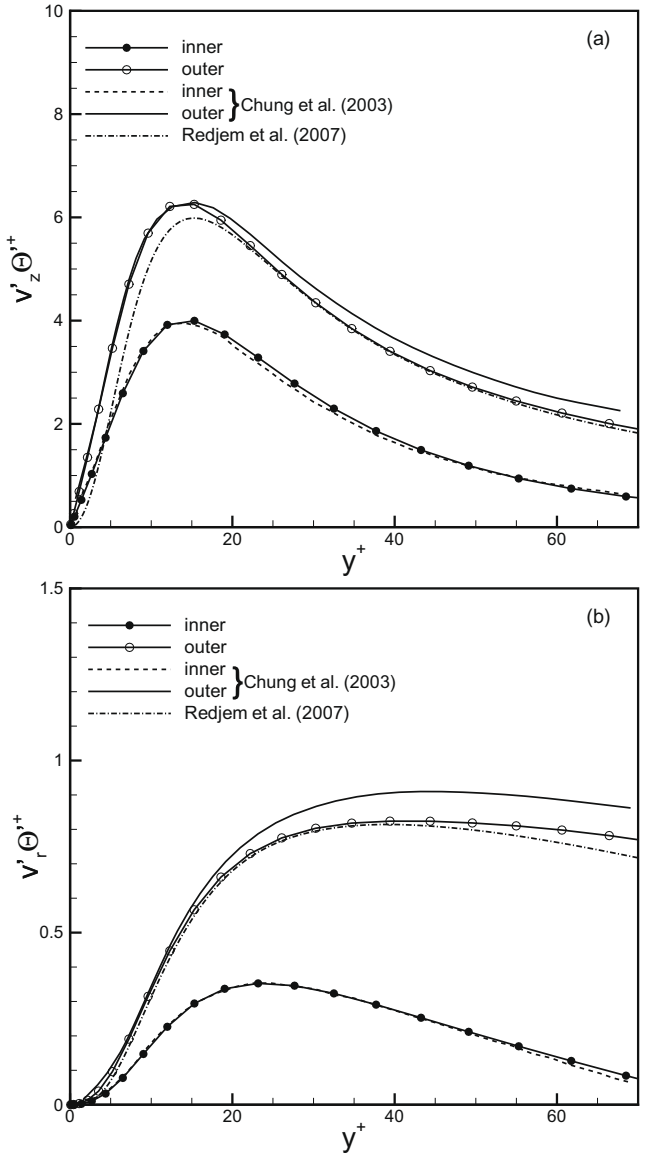

Fig. 10. Turbulent heat fluxes for $q^* = 1$. (a) streamwise component and (b) wall-normal component.

The streamwise turbulent heat flux is shown in Fig. 11 for various values of the heat flux ratio. When q^* varies from 1 to 0.01, there is a noticeable reduction of the streamwise turbulent heat flux close to the inner tube, while it undergoes a slight changes close to the outer tube. These results suggest that, for the range of heat flux ratio $q^* \leqslant 1$, the heat transfer is significantly affected near the inner wall and remains nearly constant near the outer wall. On the contrary, for $q^* > 1$, the streamwise heat flux is more intense close to the inner cylinder, and this tendency is more distinct with increases in q^* values. A variation in q^* from 1 to 100 leads to a sharp rise of the maximum in the streamwise heat flux at the inner side. The maximum is reduced at the outer side and tends to zero close to the outer wall for $q^* = 100$. For this range of heat flux ratios, $q^* > 1$, the heat transfer is thus affected both at inner and outer walls of the annular space.

Fig. 12 illustrates the distribution of the wall-normal (radial) turbulent heat flux normalized by friction velocity and friction temperature, for heat flux ratio ranges $q^* \leqslant 1$ (Fig. 12a) and $q^* \geqslant 1$ (Fig. 12b). In case of equal uniform heat fluxes on both walls ($q^* = 1$), the wall-normal turbulent heat flux profile is asymmetric, like the Reynolds shear stress profile is. The position of the zero wall-normal heat flux is $y^* = y/\delta = 0.46$ and it is closer to the inner surface than is the position of the zero Reynolds shear stress, $y^* = 1.39$.

When varying the heat flux ratio from $q^* = 1$ to $q^* = 0.01$, Fig. 12a shows that the radial heat flux is gradually attenuated in the vicinity of the inner wall and its peak disappears for the smallest values of q^*. Close to the outer wall, the peak is nearly insensitive to the diminution in q^* although a slight augmentation can be seen. The wall-normal heat flux values are more intense near the outer side like the rms temperature fluctuation profiles and like the streamwise heat flux distributions. It is notable that the position of zero radial heat flux moves towards the inner wall when q^* decreases, until the wall-normal heat flux vanishes on the inner wall for $q^* = 0.01$.

On the contrary, the differences in wall-normal heat flux level close to the inner cylinder are more significant when q^* increases from 1 to 100, as can be seen in Fig. 12b. The augmentation in q^* seems to compensate for the difference between the inner and outer cylinder areas. The position of zero radial heat flux shifts towards the outer cylinder when q^* increases, revealing that the heat transfer normal to the walls goes mainly from the inner to the outer wall.

Fig. 13 shows the dimensionless position of zero wall-normal turbulent heat flux, $y^* = y/\delta$, versus the heat flux ratio q^*. Two distinct evolutions of this position are clearly displayed: for $q^* \leqslant 1$, the position y^* develops as the power law $y/\delta = 0.46q^{*0.53}$ (which is the best fit of this evolution) while it deviates significantly from this law for $q^* > 1$.

One of the major difficulties in studying turbulent annular pipe flows is the estimation of the ratio of the shear stresses on the two surfaces, and the related problem of evaluating the radial position of maximum streamwise velocity, r_{max}, and the radial position of zero shear stress, r_0. In many previous work reported in the literature, these two positions were assumed to be equal ($\xi = r_{max} = r_0$). By this way, the ratio of shear stresses is easily derived as a function of ξ for fully developed flow, allowing thus to establish the shear stress distribution, the velocity and eddy viscosity profiles. It was also assumed in these models that the eddy viscosity equation could be used directly for determining the thermal eddy diffusivity. The shear stress distribution was a prequisite to calculate heat transfer, since a heat and momentum analogy method was used.

Based on an intensive experimental work, Rehme (1974) showed that the positions of zero shear stress and maximum velocity do not coincide. Therefore, the concept of eddy viscosity cannot be suitably applicable for annular flows. The concept of mixing length, the semi-empirical equations of conservation for the kinetic energy turbulence and the rate of dissipation of turbulence are also precluded for an annular flow. More recently, Kaneda et al. (2003) employed the semi-empirical analytical solutions obtained by Churchill and Chan (1995a,b) and Churchill (1997) for circular tube and parallel-plate channels, who extended these solutions to the annular pipe flow by introducing some modifications. Zeng et al. (2007) proposed a mathematical model (semi-empirical–integral method) for fully developed turbulent heat transfer in narrow annuli. To our best knowledge, there is no complete analysis of this problem in the archival literature. In this context, DNS of turbulent heat transfer and fluid flow in an annular duct appears to be an inestimable resource to determine: (1) the velocity and temperature profiles, (2) the positions of maximum and zero shear stress, (3) the shear stress distribution which is extremely difficult to measure directly, and (4) the friction and heat

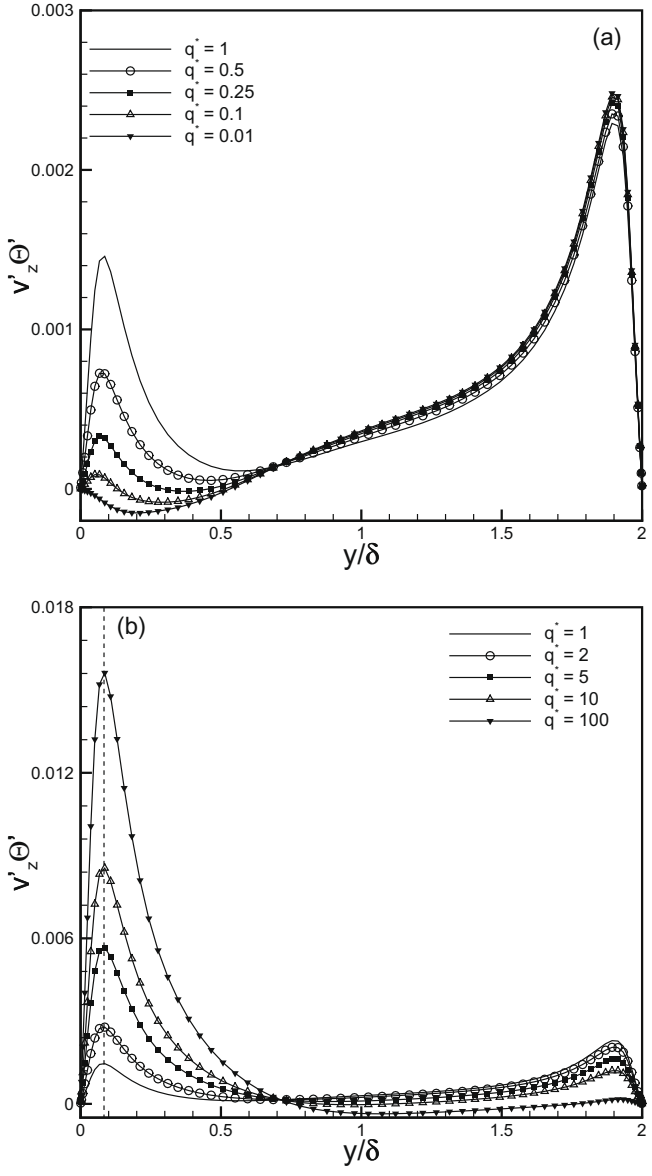

Fig. 11. Streamwise turbulent heat flux for various heat flux ratios. (a) $q^* \leqslant 1$ and (b) $q^* \geqslant 1$.

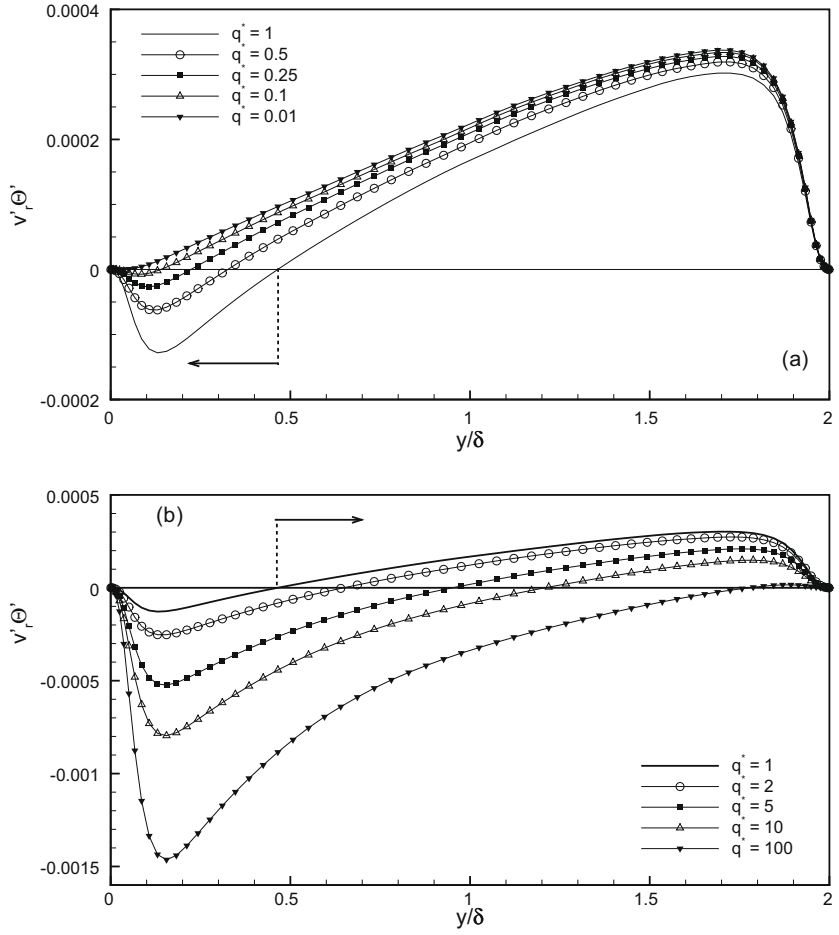

Fig. 12. Wall-normal turbulent heat flux for various heat flux ratios. (a) $q^* \leqslant 1$ and (b) $q^* \geqslant 1$.

transfer coefficients. Based on DNS predictions, one can derive well appropriate correlation equations for the turbulent velocity and shear stress profiles in annular space, and thus develop more accurate turbulence models.

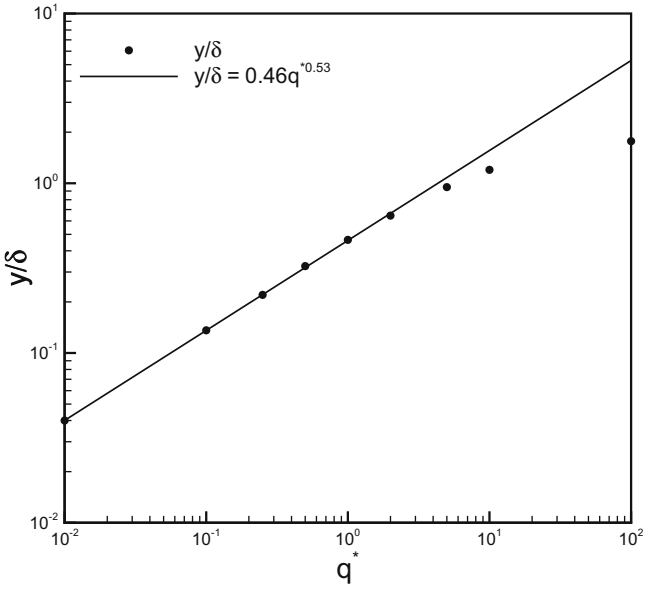

Fig. 13. Position of zero wall-normal turbulent heat flux versus heat flux ratio.

3.7. Nusselt number

A literature survey reveals that investigations on the effect of heat flux ratio on turbulent heat transfer in annular spaces with arbitrary prescribed heat flux are very few, and when available, are incomplete and uncertain. The present results were thus validated through comparisons with those reported in the case $q^* = 1$, only.

The Nusselt numbers based on the hydraulic diameter are listed in Table 2 for several heat flux ratios q^*. Nu_1 and Nu_2 stand for the inner and outer wall values, respectively. For $q^* = 1$, the predicted values $Nu_1 = 60.2$ and $Nu_2 = 26.1$ are consistent with the DNS data of Chung and Sung (2003) who reported $Nu_1 = 62.53$ and $Nu_2 = 27.63$. The diminution in heat flux ratio from 1 to 0.01 results in a substantial reduction in heat transfer at the inner wall. On the outer cylinder, Nu_2 increases slightly. The imposed heat flux

Table 2
Effect of heat flux ratio on inner and outer Nusselt numbers.

q^*	Nu_1	Nu_2
0.01	0.27	28.1
0.1	2.92	27.5
0.25	8.01	27.3
0.5	18.94	26.8
1	60.2	26.1
2	62.3	24.3
5	65.8	20.6
10	70.7	12.4
100	75.1	5.6

on the inner tube has a weak influence on the heat transfer at the outer wall because of the small radius ratio considered. When q^* varies from 1 to 100, the Nusselt number is enhanced at the inner wall while it undergoes a significant decrease at the outer wall for the largest value of q^*.

4. Conclusion

Direct numerical simulation of the fully developed turbulent flow and heat transfer in a pipe of annular cross-section, with arbitrarily prescribed heat fluxes on the walls, has been performed.

The present DNS predictions of the flow field are in good agreement with the results of literature. Close to the outer surface, the viscous sublayer, the buffer and logarithmic regions are clearly distinguished on the mean streamwise velocity profiles. At the inner surface, the velocity distribution deviates from the logarithmic law. Due to the curvature effect, the rms of velocity fluctuations and the Reynolds shear stress $\overline{v_z' v_r'}$ near the outer cylinder are more intense than those near the inner one.

The main emphasis has been placed on the effect of the heat flux ratio $q^* = q_1/q_2$ on turbulent thermal fields. For $q^* = 1$, the present calculations agree with results reported in the literature. The rms of temperature fluctuations near the outer wall of the annulus are larger than those at the inner wall, like the turbulent heat fluxes. The surface of the outer cylinder being larger than the inner one produces more heat.

In the vicinity of the walls, when q^* varies, the mean temperature distribution develops asymptotically as $\Theta^+ = Pry^+$, in the conductive sublayer, irrespective of the heat flux ratio. Beyond this sublayer, the turbulent thermal field is clearly affected by the heat flux ratio. For $q^* = 0.01$, the buffer and logarithmic regions are practically non-existent near the inner wall, while they are better distinguishable for the highest heat flux ratio ($q^* = 100$). The opposite trend is seen in the vicinity of the outer wall. For $q^* = 1$, the inner and outer Nusselt number values are consistent with those predicted by Chung and Sung (2003).

When the heat flux ratio decrease from 1 to 0.01, the temperature fluctuation intensities, the wall-normal and streamwise turbulent heat fluxes and the Nusselt numbers are reduced near the inner wall, whereas they change slightly near the outer wall. When the heat flux ratio increases from 1 to 100, the opposite trends are observed: there is a substantial enhancement of the thermal statistics (temperature fluctuation intensities and turbulent heat fluxes) close to the inner wall. An augmentation in the inner Nusselt number is seen, while a reduction in the outer Nusselt number is found.

The position of the zero radial turbulent heat flux shifts towards the inner wall, until the radial heat flux vanishes at the inner wall, for $q^* = 0.01$. For the ratios $q^* \leqslant 1$, a power law correlation is proposed: $y/\delta = 0.46 q^{*0.53}$. The present DNS predictions will be helpful for developing more accurate turbulence models for heat transfer and fluid flow in annular ducts with arbitrarily prescribed heat fluxes on the walls.

References

Chung, S.Y., Sung, H.J., 2003. Direct numerical simulation of turbulent concentric annular pipe flow. Part II: Heat transfer. Int. J. of Heat and Fluid Flow. 24, 399–411.

Chung, S.Y., Rhee, G.H., Sung, H.J., 2002. Direct numerical simulation of turbulent concentric annular pipe flow. Part I: Flow field. Int. J. Heat Fluid Flow. 23, 426–440.

Churchill, S.W., 1997. New simplified models and formulations for turbulent flow and convection. AIChE J. 43 (5), 1125–1140.

Churchill, S.W., Chan, C., 1995a. Theoretically based correlating equations for the local characteristics of fully turbulent flow in round tubes and between parallel plates. Ind. Eng. Chem. Res. 34 (4), 1332–1341.

Churchill, S.W., Chan, C., 1995b. Turbulent flow in channels in terms of local turbulent shear and normal stresses. AIChE J. 41 (12), 2513–2521.

Kaneda, M., Yu, B., Ozoe, H., Churchill, S.W., 2003. The characteristics of turbulent flow and convection in concentric circular annuli. Part I: flow. Int. J. Heat Mass Transfer 46 (26), 5045–5057. 114, 598–606.

Kays, W.M., Leung, E.Y., 1963. Heat transfer in annular passages – hydrodynamically developed turbulent flow with arbitrarily prescribed eat flux. Int. J. Heat Mass Transfer 6, 537–557. 114, 598–606.

Kim, J., Moin, P., Moser, R., 1987. Turbulence statistics in fully developed channel flow at low Reynolds number. J. Fluid Mech. 177, 133–166.

Kong, H., Choi, H., Lee, J.S., 2000. Direct numerical simulation of turbulent thermal boundary layers. Phys. Fluids 12, 2555–2568.

Lu, D.M., Hetsroni, G., 1995. Direct numerical simulation of turbulent open channel flow with passive heat transfer. Int. J. Heat Mass Transfer 38, 3241–3251.

Redjem-Saad, L., 2008. Simulation numérique des transferts de chaleur turbulents par convection forcée dans les conduites cylindriques et les espaces annulaires. Ph.D. Thesis, Université Paris-Est.

Redjem-Saad, L., Ould-Rouiss, M., Lauriat, G., 2007. Direct numerical simulation of turbulent heat transfer in pipe flows: effect of Prandtl number. Int. J. Heat Fluid Flow 28 (5), 847–861.

Rehme, K., 1974. Turbulent flow in smooth concentric annuli with small radius ratios. J. Fluid Mech. 64, 263–287.

Tiselj, I., Bergant, R., Mavko, B., Baisic, I., Hetsroni, G., 2001. DNS of turbulent heat transfer in channel flow with heat conduction in the solid wall. Trans. ASME: J. Heat Transfer 123, 849–857.

Yu, B., Kawaguchi, Y., Kaneda, M., Ozoe, H., Churchill, S.W., 2005a. The computed characteristics of turbulent flow and convection in concentric circular annuli. Part II. Uniform heating on the inner surface. Int. J. of Heat Mass Transfer 48, 621–634. 114, 598–606.

Yu, B., Kawaguchi, Y., Ozoe, H., Churchill, S.W., 2005b. The computed characteristics of turbulent flow and convection in concentric circular annuli. Part III. Alternative thermalboundary conditions. Int. J. Heat Mass Transfer 48, 635–646.

Zeng, H.Y., Qiu, S.Z., Jia, D.N., 2007. Investigation on the characteristics of the flow and heat transfer in bilaterally heated narrow annuli. Int. J. Heat Mass Transfer 50, 492–501.